Effects of anodizing surface treatment on the mechanical strength of aluminum alloy 5083 to fibre reinforced composites adhesive joints

V. Fiore, F. Di Franco*, R. Miranda, M. Santamaria, D. Badagliacco, A. Valenza

Department of Engineering, University of Palermo

Viale delle Scienze, Edificio 6, 90128 Palermo, Italy

Email: francesco.difranco@unipa.it

*Corresponding Author

Abstract

In this study, the anodizing process based on the use of tartaric sulfuric acid solution (TSA) was carried out on metal substrate to evaluate for the first time its effect on the adhesion strength and corrosion resistance of aluminium alloy (i.e., AA5083) to fibre (i.e., basalt or glass) reinforced composite adhesive joints for nautical applications. Furthermore, some TSA anodized samples were soaked in a NaOH solution to investigate the influence of this post-immersion step on the joint performances. With the aim to improve the fibre-matrix adhesion in the composite substrate thus further increasing the overall mechanical response of the joint, glass and basalt fibres were treated with a silane coupling agent solution. The corrosion behaviour of the aluminium alloy was studied by electrochemical techniques. Samples morphology was analysed by scanning electron microscopy, while the interaction between aluminium alloy substrate and epoxy resin was studied through contact angle analysis and resin uptake tests. The effectiveness of the silane treatment was examined by means of Fourier transform infrared spectroscopy and quasi-static tensile tests carried out on dry glass and basalt fabrics. The mechanical response of the resulting joints was evaluated by means of quasi-static tensile tests in accordance to ASTM D3528 standard.

Keywords: Adhesive Joint, Surface Treatment, Corrosion Resistance, Anodizing, Basalt, Silane Coupling Agent

1 Introduction

Joints play an important role in several industrial sectors because it is difficult or impossible to create a monolithic structure. Moreover, the increasing demand for light and strong structures leads to the use of different materials at the same time. Hence, metal alloys are widely used together with fibre reinforced polymers (FRPs) in order to obtain hybrid structures suitable for several engineering applications such as nautical, aerospace and automotive [1–3]. In the ship design for instance, the topside and the hull structures are critical from stiffness and strength point of views, respectively [4]. Hence, also depending on the boat length, high stability and good mechanical performances of the ships can be achieved by choosing high-stiffness materials such as aluminium alloy (i.e. 5000 series) and steel for the topside structures and a high-strength material such as fibre reinforced composite for the hull structures. Consequently, structural joints are required in order to link these dissimilar materials.

Composite and metal substrates can be joined mechanically [5,6], adhesively or through a combination of both techniques [7–9]. The first one uses a third component to join different substrates that could be a bolt or a rivet. It often requires the drilling of the substrates, thus creating stress concentration and damaged area. Conversely, adhesive joints present several advantages such as reduction of local delamination due to the absence of holes, significant weight and cost reduction. However, they cannot be used in structures which require subsequent disassembly for maintenance and inspection. There are two types of adhesive joints: i.e., secondary bonding, which involves an adhesive, and co-cured bonding, where, for example, a thermoset resin plays the role both of composite matrix and composite to metal adhesive at the same time [10].

The constant increase of the use of composite materials in each industrial field generates a considerable environmental concern due to the widespread use of thermoset based composites reinforced with synthetic fibres (i.e., glass, carbon and Kevlar), because there are few recycling options and also because of the use of petroleum based raw materials. To overcome this problem,

natural fibres as reinforcements and bio-thermoset resins as matrix has attracted a growing interest in the last years from industry and academia. In this context, Cicala et al. [11] developed a recyclable and bio-based epoxy formulation suitable for resin infusion by using a bio-based epoxy monomer and a cleavable ammine. Fibre reinforced laminates were manufactured through vacuum infusion process and chemically recycled in mild acetic acid aqueous solutions, thus obtaining clean fibres and a reusable thermoplastic.

As concerns the reinforcement phase, natural fibres (i.e., jute, flax, ramie, hemp and so on) are very promising due to their specific properties, low price, large availability, health advantages and sustainability. Moreover, they are renewable and have a CO_2-neutral life cycle, in contrast to their synthetic counterparts. Nevertheless, their hydrophilic nature, highly variable mechanical properties, poor adhesion with polymeric matrices as well as their lower mechanical properties in comparison to synthetic ones are the main drawbacks. Due to their mineral origin, basalt fibres represent a valid alternative to glass ones thanks to easy availability, high thermal stability, good chemical inertia and comparable mechanical properties. Furthermore, basalt is one of the most common rocks on earth, so it can be considered inexpensive and eco-friendly [12,13].

A wide literature shows that the mechanical performances of adhesive joints can be noticeably improved through surface treatments of the substrates [14–20]. The latter could be of different nature: i.e., mechanical, chemical, electrochemical, with coupling agents or laser [21]. For instance, Aghamohammadi et al. [22] evaluated the effect of four different surface treatments (i.e., mechanical abrasion with sandpaper, electrochemical treatments such as anodizing and two chemical etching) on the quasi-static flexural response of Fiber Metal Laminates (FMLs) made up of aluminium alloy 2024, basalt fibres and epoxy resin. The authors found that the anodizing process allowed to achieve the best mechanical properties of the resulting FMLs. These results were ascribed to the formation of nanoscopic pore on the metal surface, thus leading to better interlocking with the polymeric phase even if the highest roughness values were achieved through mechanical abrasion.

The anodizing is an electrochemical process that allows creating an oxide layer on the aluminium surface whose thickness and microstructure can be tuned by parameters such as time, temperature, bath composition, hydrodynamics conditions and applied voltage [23–26]. If anodizing is carried out in acidic electrolyte such as sulphuric acid, chromic acid, etc. the anodic oxide self organizes assuming a regular porous structure with an inner barrier layer (tens nm thick) and an outer porous layer (tens μm thick). The latter can be sealed to further enhance the corrosion resistance provided by the barrier layer by a simple hydration process. Zhang et al. demonstrated that using anodized aluminium for the production adhesive aluminium to composite joints enhanced their strength and corrosion resistance, since empty pores of anodic oxide absorb resin thus leading to a good mechanical interlocking [27]. However, they obtained the best results using a chromic acid bath with severe concerns about the environmental impact of Cr(VI), which is highly carcinogenic.

Thus, alternative environmental friendly chromium-free electrolytes have been proposed in the literature for anodizing aluminum alloys. Among them, one of the most promising is Tartaric Sulfuric acid solution (TSA) successfully used for anodizing of AA2024 aluminum alloy [28]. In particular, tartaric acid was added to sulfuric acid anodizing baths to generate porous anodic film that provides high corrosion resistance to these alloys due to residues of tartaric acid in the pore solution.

In this context, it is worth noting that to the best of our knowledge there are no previous papers on the improvement of the adhesion of metal to composite hybrid joints through anodic layers grown in TSA on aluminum alloys. Furthermore, the anodizing process based on TSA solution has never been used on 5000 series aluminum alloy for any of the previously described purposes. Hence, for the first time, an alternative anodizing process based on environmental friendly chromium-free electrolytes were employed to enhance the bonding strength of adhesive co-cured joints in double-strap configuration for nautical applications. Aluminium alloy 5083 is widely used in shipbuilding, due to its good corrosion resistance as well as super plastic properties that lead to an easier formability [29]. Glass and basalt fibres were chosen as reinforcement of the composite substrate to compare the

traditional and most extensively used fibre in nautical field (i.e. glass) with its most promising eco-friendly alternative (i.e. basalt) [12].

Different treatments were carried out on the aluminum alloy to analyze their influences on the bonding strength and corrosion resistance of the adhesive joints: i.e. mechanical abrasion (as reference) and anodizing in two different and innovative anodizing baths. Moreover, silane coupling agent treatment was performed on glass and basalt fibres to improve their adhesion with the epoxy matrix and, as a consequence, to achieve an overall improvement of the joint performances.

2 Experimental

2.1 Materials

Aluminium alloy 5083 with a nominal thickness of 3.5 mm was selected as the metal substrate in this study. Two woven plain weave fabrics were used as reinforcement of composite substrate: i.e., basalt with areal weight 220 g/m^2 and glass 200 g/m^2. As concerns the matrix phase, SuperSap® 300 and the cure inhibitor INH by Entropy Resins were mixed with the Recyclamine® 301 by Connora Technologies with the following mix ratios: 100:32:11 (resin: curing agent: INH) by weight.

2.2 Metal surface treatments

Two different types of treatment were carried out: i.e., mechanical abrasion (MA) and anodizing. The first one involved a mechanical abrasion phase with the aid of an orbital sander with sandpaper grit 80 and then an acetone cleaning. The joints manufactured by using mechanical abraded metal substrate was considered as reference.

For the anodizing process, the metal samples were first smoothed with sandpapers of increasing grit up to 2000 and then cleaned in an ultrasonic acetone bath. Afterwards, they were immersed in an etching 10%wt of NaOH aqueous solution, subsequently cleaned with deionized water and, after that, de-smutted in 30%v/v HNO_3 aqueous solution. Two anodizing baths were investigated: 0.48 M

sulfuric acid with the addition of 80 g/l of tartaric acid (TSA) [28] and 0.4 M phosphoric acid (PA). The process parameters are summarized in Tab. 1.

Anodizing baths	Temperature [°C]	Voltage [V]	Time [min]
TSA	37	14	20
PA	1	160	30

Tab. 1: Process parameters of anodizing treatments

After the anodizing process, the surface was dried at room temperature. Some TSA anodized samples were also etched in 0.1 M NaOH for 2 minutes in order to widen the pores of the anodic layers (TSA-NaOH).

2.3 Fibres surface treatments

An amino-silane coupling agent, the (3-Aminopropyl)trimethoxysilane (SIL), was used to increase the fibre-matrix adhesion in composite substrates [30,31]. First, basalt and glass fabrics underwent a de-sizing process in order to remove possible dirt and commercial sizing. As suggested by the literature two approaches were used: i.e., thermal treatment (TT) [32] and immersion in acetone (ACE) [33]. As concerns thermal treatment, the fabrics were heated in an oven at 350°C for 3 hours. For ACE treatment, fabrics were soaked in acetone for 24 h, then cleaned with deionized water and dried in an oven at 80 °C for 24 hours.

After the de-sizing phase, glass and basalt fabrics were subjected to a silane treatment as follows. Firstly, the solution, composed by 90%v/v of ethanol, 5%v/v of deionized water and 5%v/v of silane, was magnetically stirred at room temperature for 24 h in order to hydrolyse the silane molecules to form silanol groups, while the pH was adjusted to 4.3 by adding acetic acid [34]. Then, fabrics were immersed for 2 hours in the solution and, finally, dried in an oven at 80 °C for 24 hours.

2.4 Joints manufacturing

Double strap joints were manufactured through vacuum infusion process, cured for 24 hours at room temperature and then post-cured for 3 hours at 100 °C. In particular, two metal substrates (110 mm x 160 mm) were placed side by side (i.e., in contact with each other) in a plain mold and twelve dry glass or basalt fabrics (50 mm x 160 mm) were located in correspondence of the overlap area (i.e., six above and six below the metal substrates as shown in Fig. 1). Afterwards, the mold was compacted by a vacuum bag and then the fabrics were impregnated by resin, which flows through, mainly driven by the applied vacuum. After the curing process, each resulting panel (160 mm width, 220 mm length) was cut with a rotating blade to obtain five specimens having width equal to 25 mm for each condition.

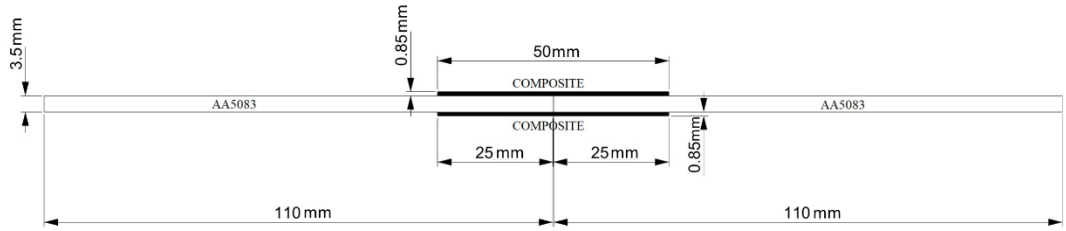

Fig. 1: Tensile testing sample section

2.5 Quasi-static tensile tests

Five samples for each condition were tested in tensile configuration according to ASTM D3528 standard by using an electromechanical testing machine WANCE model ETM-C, equipped with a load cell of 50 kN. The crosshead speed was set equal to 1.27 mm/min. The strain of the specimens was evaluated trough a YYU-10/50 extensometer with a gauge length of 50 mm and a full-scale value equal to 20% coupled to the testing machine.

The shear strength of the joint was calculated by the equation:

$$Joint\ shear\ strength = \frac{P_{max}}{2A} \quad (1)$$

Where P_{max} is the maximum load and A is the overlap area. For sake of simplicity, peel stresses were neglected here.

Furthermore, three glass and basalt dry fabrics (180 mm x 30 mm) for each condition were tested in tensile configuration in order to evaluate the influence of the de-sizing process on their mechanical performances. In particular, tensile tests were carried out on "as supplied" (AS), "pre-treated" (i.e. TT and ACE) and "silane treated" fabrics.

2.6 Analysis of the treated surfaces

The surface of electrochemically treated aluminium was observed by a Philips XL30 ESEM scanning electron microscope coupled with EDX equipment to evaluate the presence and the dimension of pore generated by the anodizing process.

In order to evaluate the chemical affinity between the anodic layer and the resin, the contact angle of a drop of resin on the top of aluminium alloy substrate was measured using *ImageJ* software. Four samples were analysed for each treatment.

Furthermore, the resin entrapped inside the pores of the anodized aluminium alloy was estimated by weighing the samples both after the deposition of a resin drop and after its removal, by using an analytical balance model AX 224 (Sartorius Italy) with high resolution (i.e., 0.1 mg). In details, the same amount of resin drop (~ 20 mg) were deposited on the sample by using a pipette and after 10 minutes, the resin drop were removed by using a lab spatula prior to weight the sample for evaluating the resin entrapped in the oxide pores. Four samples were weighted for each treatment. The resin uptake was evaluated using the following equation:

$$R_{up} = \frac{W_{with\ drop} - W_{without\ drop}}{S} \quad (2)$$

where $W_{with\ drop}$ and $W_{without\ drop}$ are the weight of the sample before and after the removal of resin drop, respectively, and S is the area where the resin was trapped.

Fourier transform infrared spectroscopy (FT-IR) analysis was carried out by using Perkin Elmer spectrometer model Spectrum II to evaluate the presence of functional groups typical of amino-silane on the fabrics surface as well as to verify the correct removal of commercial sizing. The transmittance spectrum was recorded in the frequency range of 450–4000 cm^{-1} with a resolution of 4 cm^{-1}.

2.7 Corrosion test

The corrosion behaviour of the specimens was studied by open circuit potential (OCP) measurements and electrochemical impedance spectroscopy (EIS) using a Parstat 2263 (PAR) controlled by Electrochemistry Power Suite software. The samples were dipped in 3.5%wt NaCl aqueous solution and in a three electrode cell, where the aluminium coupon was the working electrode, a Pt net was used as counter electrode and a silver/silver chloride electrode (0.197 V vs. SHE) was used as reference. Electrochemical Impedance spectra were recorded by imposing a sinusoidal stimulus of 10 mV amplitude with a frequency ranging from 0.1 Hz to 100 kHz and the resulting spectra were fitted using Zsimp software. All measurements were carried out at room temperature and under atmospheric pressure.

3 Results and discussion

3.1 Metal surface treatments

Fig. 2a shows the current density vs time curve recorded during the potentiostatic anodizing of AA5083 in TSA (see Tab. 1). The high imposed potential allows the growth of coarse pores during the anodizing process more suitable to host the epoxy resin used as adhesive of the joint as well as composite matrix [35]. The current response presented in Fig. 2 (a) indicates that during the potentiostatic hold, the current density reaches a value of ~ 11 $mA \cdot cm^{-2}$, and the circulated charge is around 13 $C \cdot cm^{-2}$. A lower value (~ 30 $\mu A \cdot cm^{-2}$) is reached during the anodizing in phosphoric acid and the circulated charge is roughly around 0.1 $C \cdot cm^{-2}$ (Fig. 2 (b)), thus much lower than that necessary in TSA even if the process conditions are more severe (i.e., 160 V at 1°C).

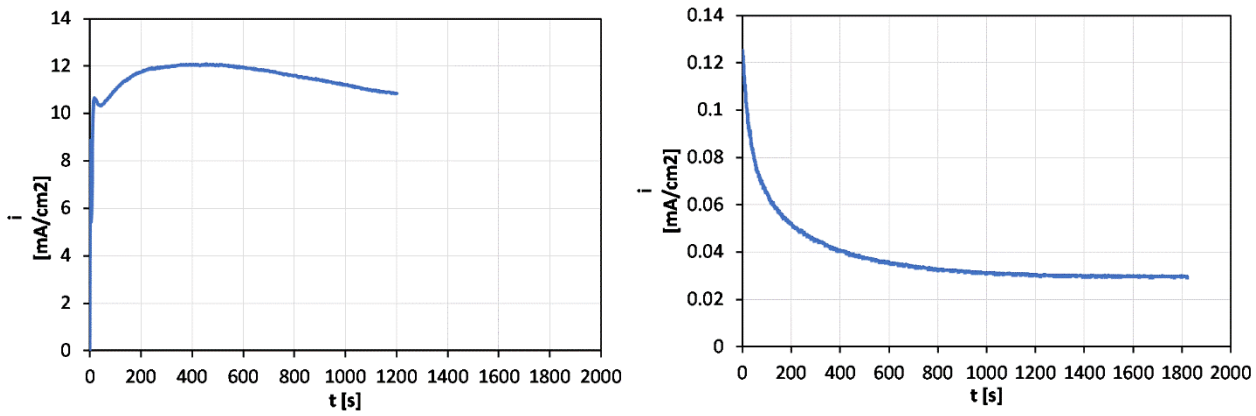

Fig. 2: Current density vs time during anodizing in different bath: (a) TSA and (b) PA.

According to SEM micrographs showing the surface of the anodized alloy, the pores have very small diameters (in the order of a few nm), that can be slightly widened by an alkaline etching in NaOH solution (compare Fig. 3 (a) and Fig. 3 (b)). If the anodizing is carried out in phosphoric acid solution, the pores are significantly larger than those grown in TSA (see Fig. 3 (c)). In Fig. S1 are shown SEM micrographs at lower magnification.

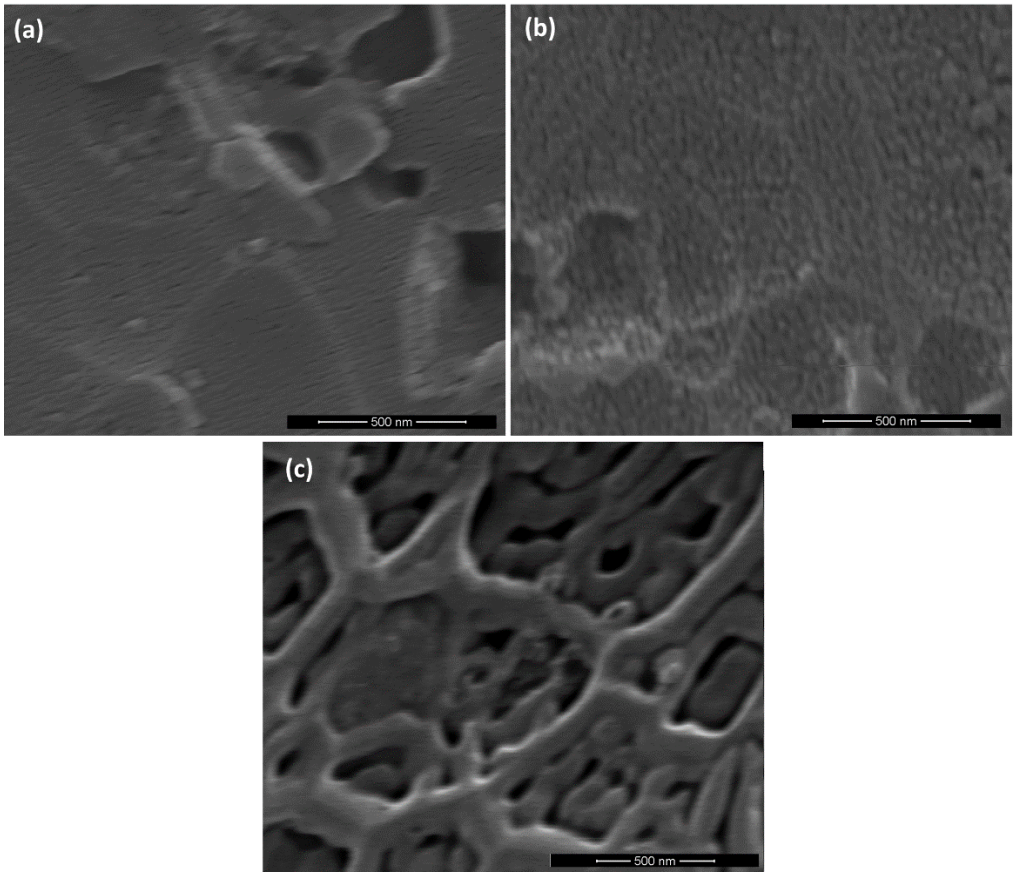

Fig. 3: SEM micrographs of Al 5083 surface after anodizing in (a) TSA, (b) TSA-NaOH and (c) PA

Fig. 4 reports the average contact angle between the resin drop and the surface of mechanically sanded and anodized Al alloys. The anodizing reduces the contact angle suggesting an improved wettability of the substrate, i.e. the presence of the porous layer enhances the chemical affinity between the substrate and the resin. Notably, the lowest contact angle was measured for the alloy anodized in TSA probably due to tartrate ions (namely $C_4H_4O_6^{2-}$) contained inside the oxide incorporated during the anodizing process [26]. This result is in agreement with the dependence of the resin uptake as a function of the surface treatment (see Fig. 5). The anodizing in phosphoric acid does not provide a significant increase of the resin uptake with respect to the mechanically sanded alloy. Conversely, anodizing in TSA allows to double the resin uptake of the alloy, and pore widening due to the alkaline etching enhances of 300% the resin uptake. Thus, matching the improved chemical affinity between the substrate and the oxide with the pore widening is a promising strategy to improve the joint performance.

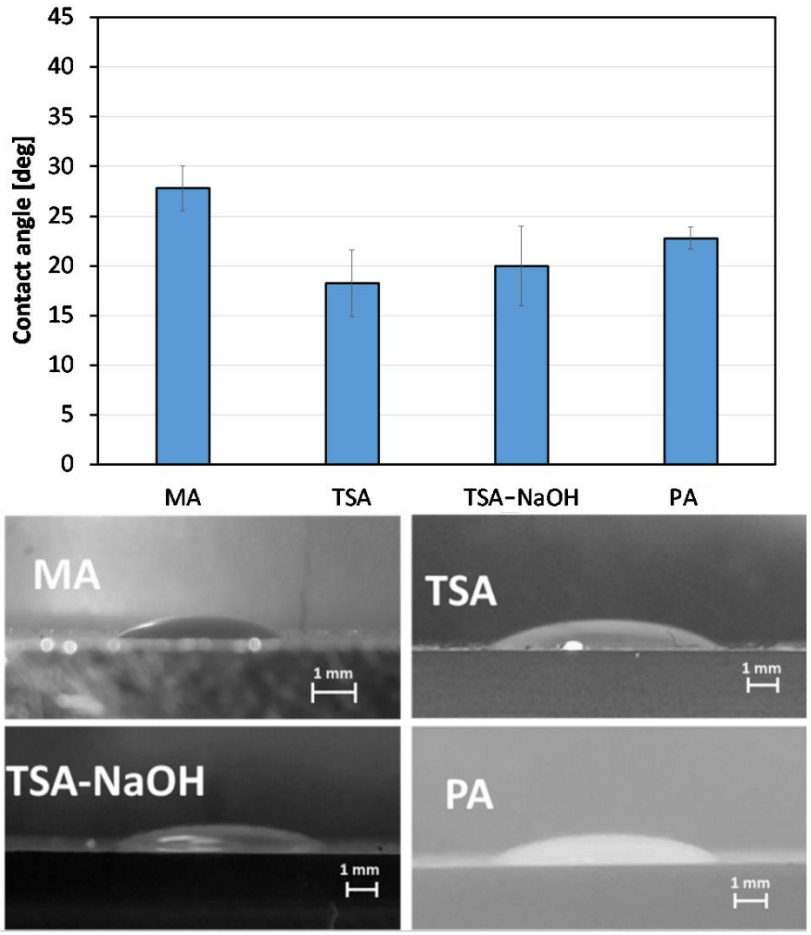

Fig. 4: Contact angle values at varying metal treatment

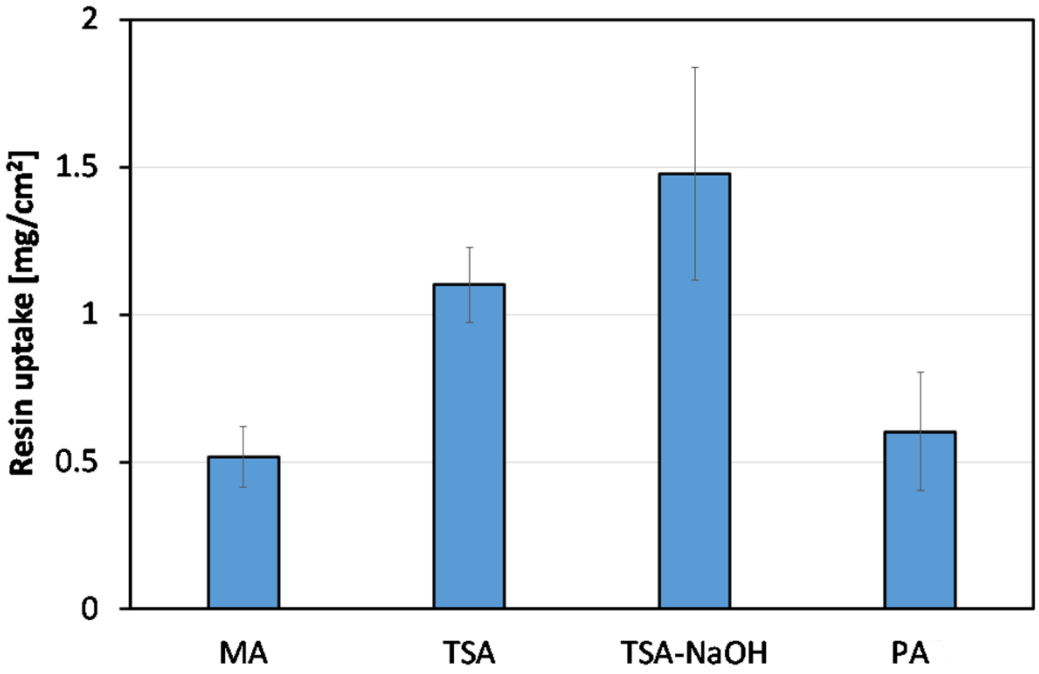

Fig. 5: Resin uptake values at varying metal treatment

The effect of surface treatment on the corrosion resistance of AA 5083 was studied in highly aggressive 3.5% NaCl solution by measuring the open circuit potential and by recording electrochemical impedance spectra. Fig. 6 shows the OCP vs time curves for mechanically polished as well as anodized alloys. The behaviour of OCP vs. time curves can be explained by considering the oxide porosity for each substrate surface treatment as well as the thickness of the barrier layer beneath. The most negative value was measured for MA due to the presence of a poorly passivated surface. More positive values were measured for anodized alloys due to the presence of the anodic oxide. Wider pores and thinner barrier layer (TSA-NaOH and PAA), helps chlorides diffusion and loss of passivity efficacy. The corresponding EIS spectra (recorded at OCP) are reported in the Nyquist representation in Fig. 7. They look like depressed semicircles with a diameter changing of several orders of magnitude. This statement can be better appreciated by fitting the spectra according to the equivalent circuit of Fig. 7, where R_{el} is the electrolyte resistance, R_p, the polarization resistance and Q_{ox} is a Constant Phase Element (CPE) introduced to model the non-ideal capacitance of the anodic oxide. The polarization resistance of Al 5083 anodized in TSA is 2-3 orders of magnitude

higher than that estimated for MA alloy, because the latter led to a poor quality and rough surface [22]. Moreover, after alkaline etching in NaOH, R_P remains significantly higher (see Tab. 2).

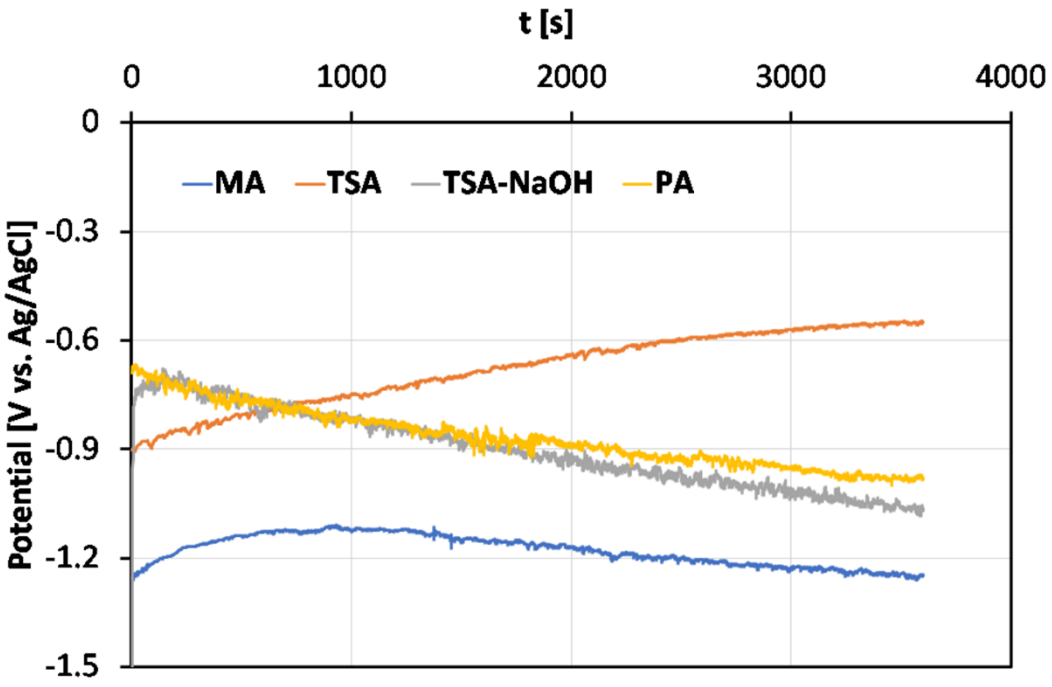

Fig. 6: OCP vs time

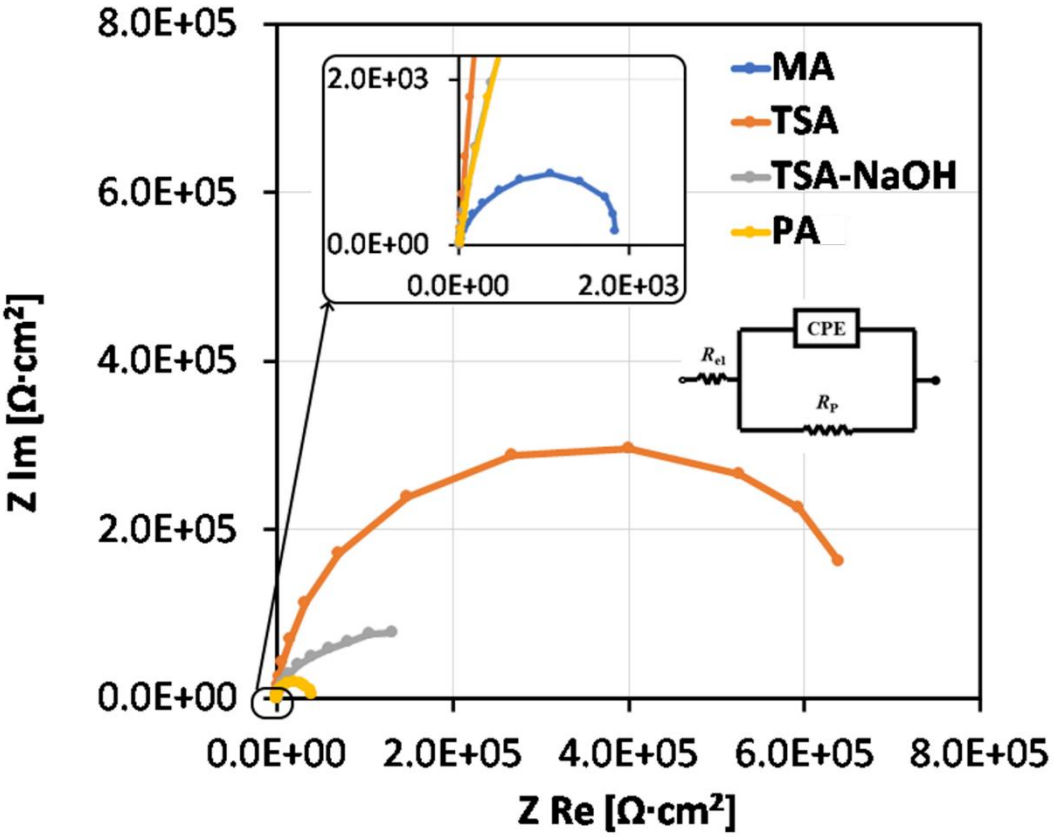

Fig. 7: Nyquist diagram and the equivalent circuit

	R_{el} [Ω cm^2]	Q_{ox} [S s^n cm^{-2}]	n	R_p [Ω cm^2]	χ^2
MA	17	5.0×10^{-5}	0.93	1950	2.3×10^{-3}
PA	18	2.0×10^{-7}	0.92	4.0×10^{4}	8.3×10^{-4}
TSA	18.5	1.0×10^{-6}	0.94	6.7×10^{5}	3.5×10^{-3}
TSA-NaOH	13.2	2.5×10^{-6}	0.88	1.6×10^{5}	2.0×10^{-2}

Tab. 2: Fitting parameter of EIS spectra of Fig. 7 according to equivalent circuit

3.2 Mechanical properties of the joints with treated metal

According to the results relating to the metal surface treatments (see section 3.1), anodizing in PA was excluded due to the poor corrosion resistance and the low resin uptake. Hence, only anodizing in TSA (without and with a post-immersion step in NaOH solution) was selected to improve the mechanical performance of the joints whereas mechanical abrasion (MA) was carried out as reference treatment. Fig. 8 compares the average values (and related standard deviation) of the joint shear strength of the specimens at the different metal treatments.

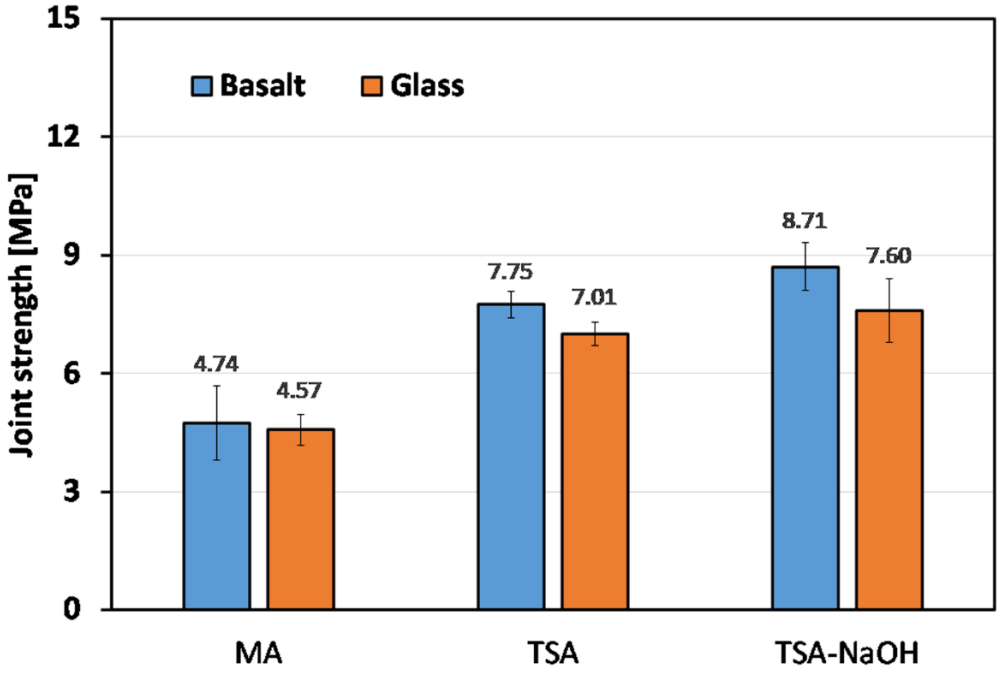

Fig. 8: Joint shear strength at varying metal treatment

The results of the tensile test confirm that the anodizing in TSA allows to noticeably improve the shear strength of the joint compared to the reference MA joints (i.e. +63.4% and +54% for basalt and glass samples, respectively). Furthermore, the post-immersion in NaOH represent a useful step, leading to further improvements of tensile strength equal to + 83.7% and + 66.3%, for basalt and glass samples, respectively.

These increments can be explained by taking into account the observed failure modes that are quite similar in joints with basalt and glass fibres. It can be evidenced that the failure mode experienced by the MA joints is adhesive (Fig. 9 (a)). In particular, only small traces of resin are visible on the metal surface, thus explaining the quite low adhesion resistance of these joints. On the contrary, TSA joints failed by partially cohesive mechanism, due to the adhesion improvement caused by the anodizing treatment. Indeed, as clearly shown in Fig. 9 (b), a greater amount of resin remains homogeneously distributed on the aluminum surface, for both kinds of joints.

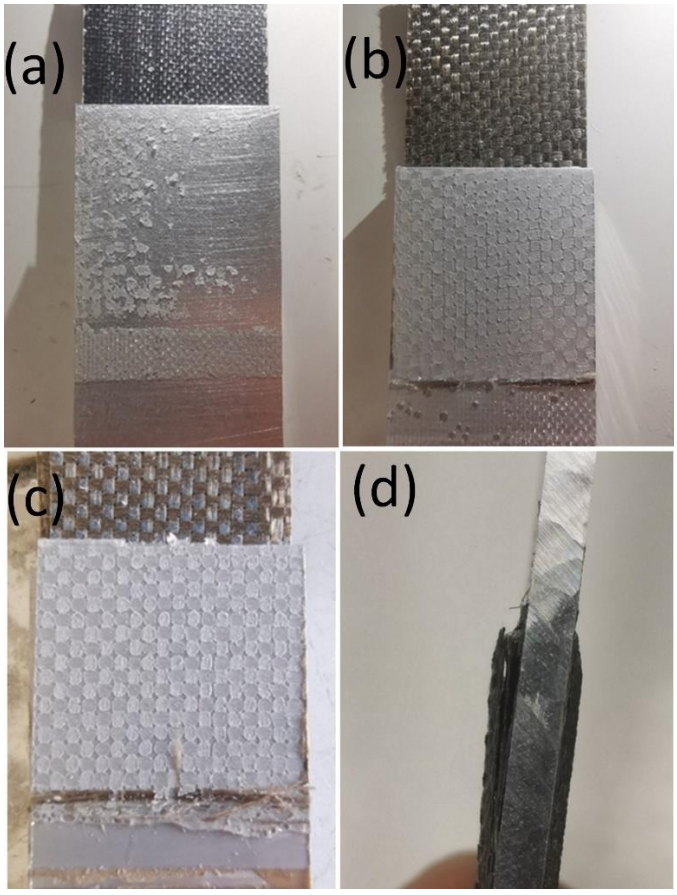

Fig. 9: Typical fracture surfaces of basalt joints: (a) MA, (b) TSA (c) TSA-NaOH and (d) TSA-NaOH with delamination

As previously stated, the best tensile performance was evidenced by TSA-NaOH samples, regardless of the kind of fibre used as reinforcement of composite substrate. Indeed, the post-immersion in NaOH 0.1 M solution of the aluminium substrate allows to further improve the strength of the joint: i.e., the failure mode became fully cohesive, as shown by the homogeneous resin layer clearly visible on the metal surface (Fig. 9 (c)). This achievement can be addressed to the pores widening effect due to the post-immersion in NaOH solution, as shown by the contact angle and resin uptake results. Furthermore, it can be noted that some TSA-NaOH joints experienced delamination failure of the composite substrate (Fig. 9 (d)). This experimental evidence is quite noteworthy because it means that, through the anodizing treatment in TSA followed by the post-immersion step in NaOH, the composite substrate became the weakest point of the joint, due to the noticeable increase of the metal to composite adhesion.

3.3 Fibres surface treatments

Typical load vs displacement curves for each kind of fabric are shown in Fig. 10. In particular, as previously written, codes "AS", "TT" or "ACE" will be used to identify as supplied, thermally treated or soaked in acetone fabrics, respectively. Furthermore, these codes were coupled with the suffix "SIL" if the silane treatment was performed.

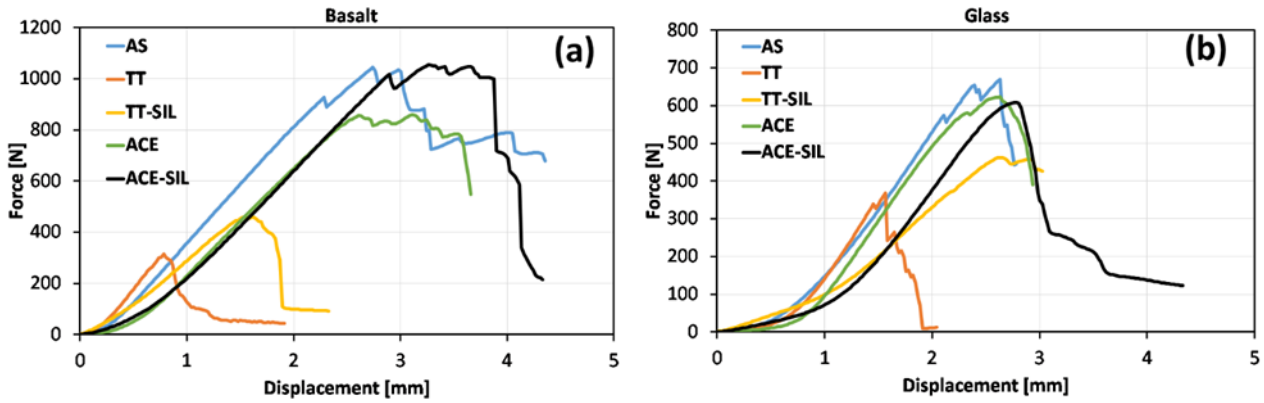

Fig. 10: Typical load vs displacement curves for (a) basalt and (b) glass fabrics

It is worth of noting that, regardless of the kind of fibre (i.e., basalt or glass), the thermal treatment significantly reduces the fabric tensile strength. Conversely, the acetone treatment does not affect it. As suggested by literature [36–38], thermal treatment correctly removes the sizing but it also could lead to the thermal degradation of the fibres. Furthermore, tensile strength reduction can occur because the removal of the organic layer exposes the defects of the fibres. This contribution can be recovered by carrying out the silane treatment that allows the covering of preexisting defects. On the contrary, the acetone treatment does not affect fibres strength, but it does not properly remove the whole commercial sizing, as reported in previous papers [39,40].

In Fig. 11 are shown the SEM micrographs relating to the fabrics with and without de-sizing process.

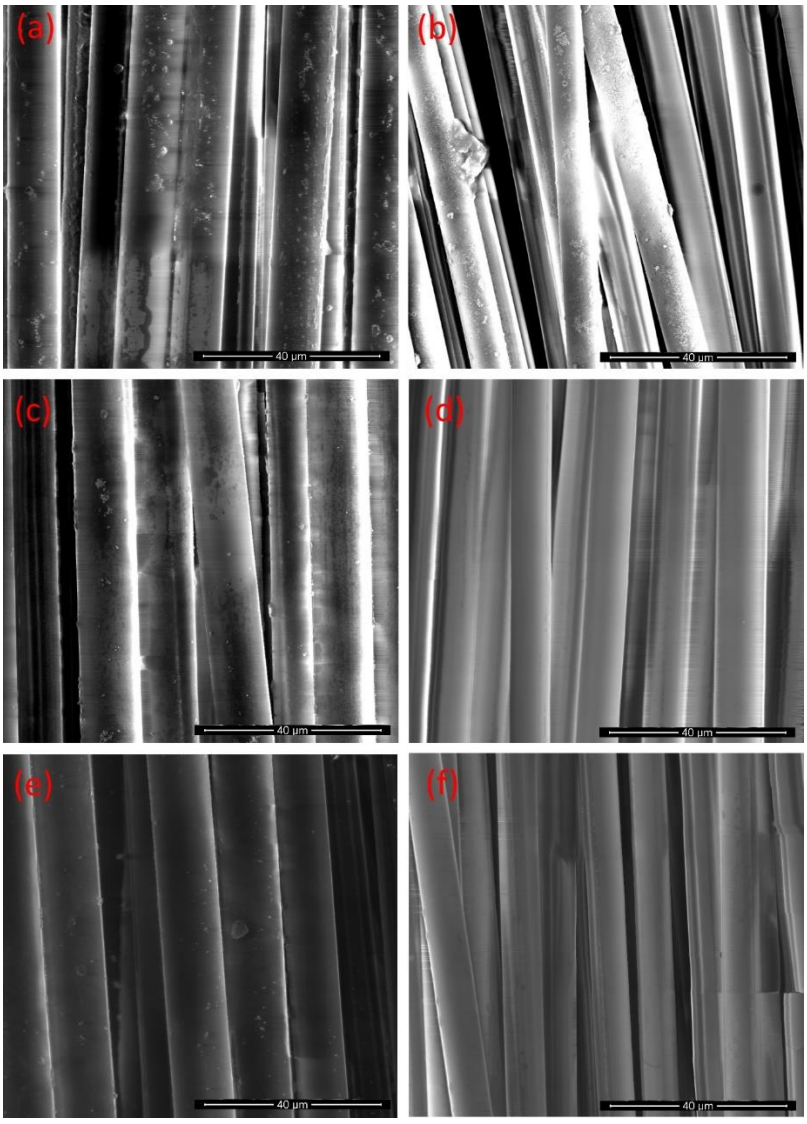

Fig. 11: SEM micrographs of fabrics with and without de-sizing process: (a) basalt-AS; (b) glass-AS; (c) basalt-TT; (d) glass -TT; (e) basalt -ACE; (f) glass -ACE

It can be observed that the fibres surface of as supplied basalt and glass appears with high roughness due to the presence of an inhomogeneous sizing layer along the fibres. After both treatments (Fig. 11c-f) the surface of fibres appears smoother, indicating that de-sizing processes are effective.

Fig. 12 shows the SEM micrographs of the fabrics after silane treatments. It is possible to see the effectiveness of the silane treatment, since it can be observed a homogenous layer surrounding the fibres.

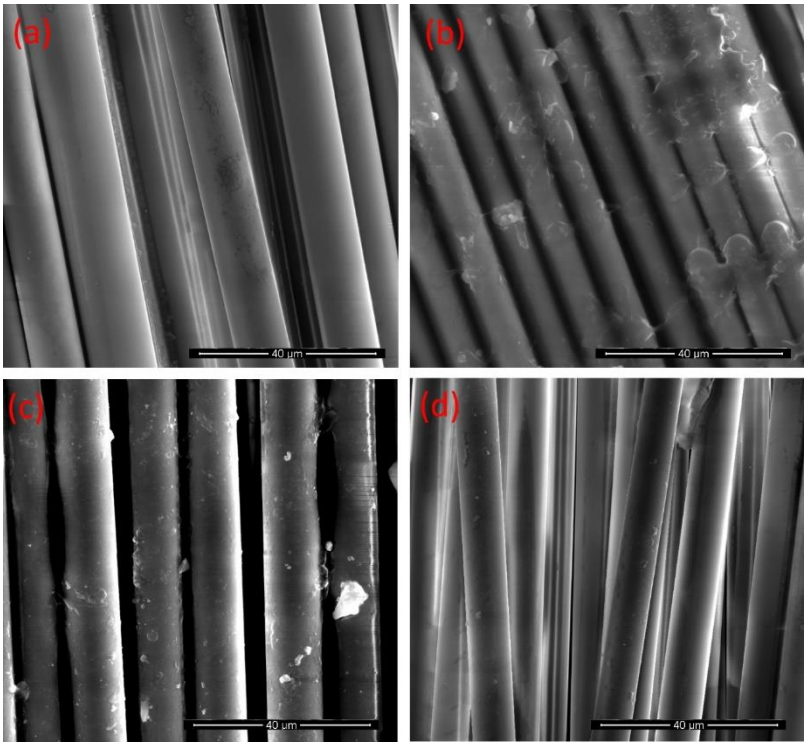

Fig. 12: SEM micrographs of fabrics after silane treatments: (a) basalt-TT-SIL; (b) glass-TT-SIL; (c) basalt-ACE-SIL; (d) glass-ACE-SIL

FTIR measurements were carried out in order to evaluate the proper removal of the organic size due to the de-sizing treatments and the chemical modifications induced by silanization (see Fig. 13).

Both basalt and glass silane treated fabrics (see Fig. 13 a and c) show major peaks centred at about 2850 and 2920 cm^{-1} that are associated with the vibration of CH_2 and CH_3 functional groups of the silane coupling agent [33]. Furthermore, the spectra of both silane treated fabrics show a wide peak centred in the range between 3200 cm-^{1} and 3500 cm^{-1}, relating to the N-H vibration stretching

[33,41]. In Fig. 13b and Fig. 13d the peaks of silane treated fabrics at 1560 cm^{-1} and 1650 cm^{-1} correspond respectively to the bending vibration of the primary amine ($-NH_2$) [42] and symmetric and asymmetric deformation vibrations from protonated amines ($-NH^+$) [33]. The peak at 1744 cm^{-1} is characteristic of the C=O stretching [43]. On the other hand, the spectra of fabrics soaked in acetone present similar (i.e. centred at same wave number) but smaller peaks in comparison to silane treated fabrics (see Fig. 13a and c), thus confirming that this treatment is not able to properly remove the commercial sizing. Conversely, the spectra of the thermal treated fabrics do not show any peak related to the amino silane groups, evidencing the total removal of the commercial sizing.

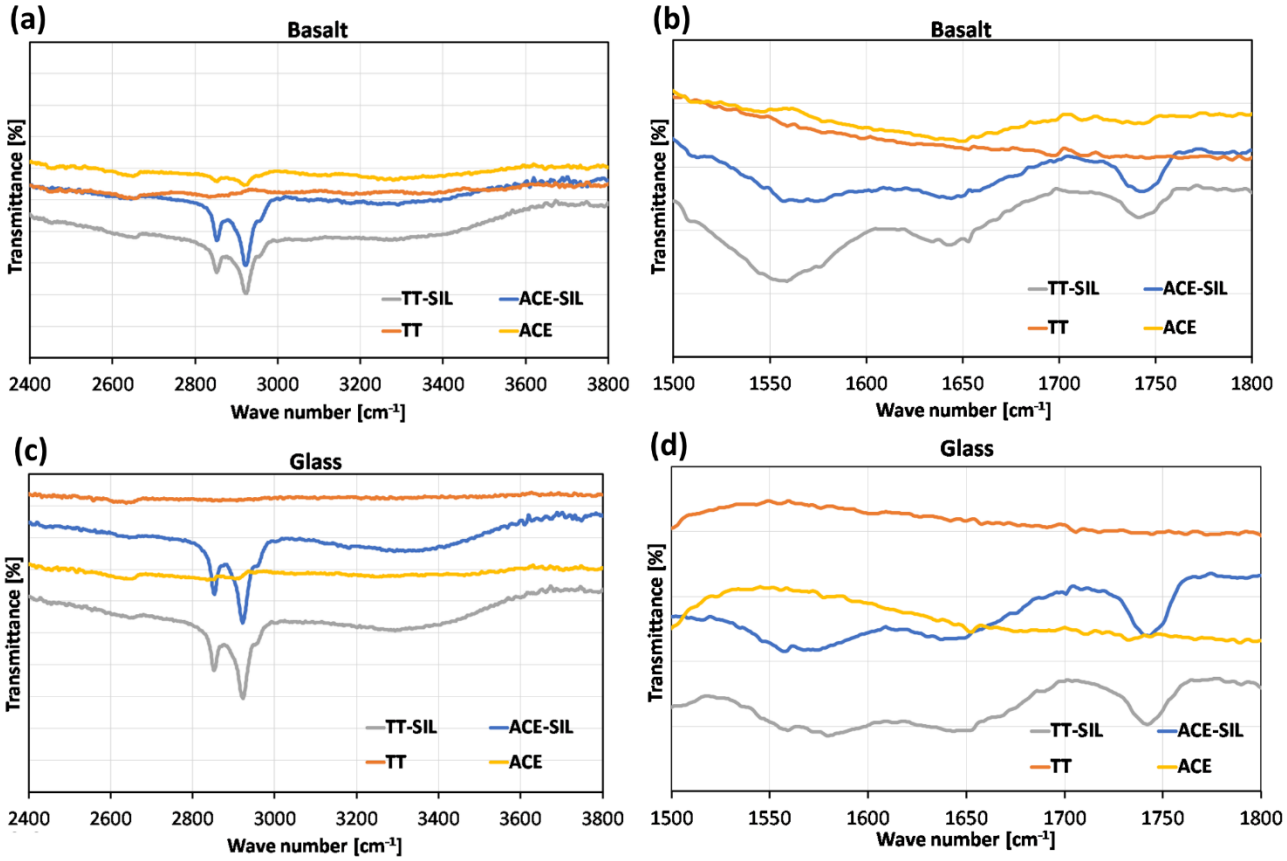

Fig. 13: FTIR spectra in two different wave number ranges of (a)-(b) basalt fabric, (c)-(d) glass fabric

3.4 Effect of silane treatment on the mechanical properties of the joints

In order to further improve the mechanical response of the joints, a silane treatment was chosen with the aim of increasing the fibre-matrix adhesion in the composite substrate. As evidenced by the results shown in section 3.2, thermal pre-treatments (TT) lead to a more significant reduction of the

mechanical strength of dry fabrics than acetone-based one (ACE). Nevertheless, the silane treatment allows to achieve an overall increase of the joints strength, as evidenced in Tab. 3. Even in this case, these improvements can be explained by observing the fracture surface of the joints.

	TSA-TT-SIL	TSA-ACE-SIL	TSA-NaOH-TT-SIL	TSA-NaOH-ACE-SIL
		Basalt		
Joint shear strength [MPa]	9.11 ± 1.17	10.87 ± 1.51	10.47 ± 0.69	11.01 ± 0.65
Increments relative to TSA [%]	+17.6	+40.3	-	-
Increments relative to TSA-NaOH [%]	-	-	+20.2	+26.3
		Glass		
Tensile strength [MPa]	8.79 ± 0.93	9.63 ± 1.08	10.61 ± 0.49	8.62 ± 0.45
Increments relative to TSA [%]	+25.4	+37.4	-	-
Increments relative to TSA-NaOH [%]	-	-	+39.6	+13.4

Tab. 3

	TSA-TT-SIL	TSA-ACE-SIL	TSA-NaOH-TT-SIL	TSA-NaOH-ACE-SIL
		Basalt		
Joint shear strength [MPa]	9.11 ± 1.17	10.87 ± 1.51	10.47 ± 0.69	11.01 ± 0.65

Increments relative to TSA [%]	+17.6	+40.3	-	-
Increments relative to TSA-NaOH [%]	-	-	+20.2	+26.3
		Glass		
Tensile strength [MPa]	8.79 ± 0.93	9.63 ± 1.08	10.61 ± 0.49	8.62 ± 0.45
Increments relative to TSA [%]	+25.4	+37.4	-	-
Increments relative to TSA-NaOH [%]	-	-	+39.6	+13.4

Tab. 3: Effect of silane treatment on joints tensile strength

By observing Fig. 14, it is worth noting that all the joints manufactured using silane treated fibres as reinforcing phase of the composite substrate showed cohesive failure mode. In more detail, Fig. 14 (a) and (b) evidence that, regardless of the kind of fabric pre-treatment (i.e., TT or ACE), some basalt fibres (with surrounding epoxy matrix) remained on TSA treated aluminium surface after joint failure, thus showing the effectiveness of the silane treatment on the fibre-matrix adhesion. Furthermore, as already evidenced for the joint without silane treatment, the post-immersion in NaOH allows to further enhance the performance of the joint. Fig. 14 (c) and (d) evidence that both joints (i.e., TSA-NaOH-TT-SIL and TSA-NaOH-ACE-SIL joints) experienced cohesive failure mode showing some traces of fibres on the metal surface. Glass joints evidenced quite similar failure modes. Hence, the related figures are not reported here for the sake of brevity.

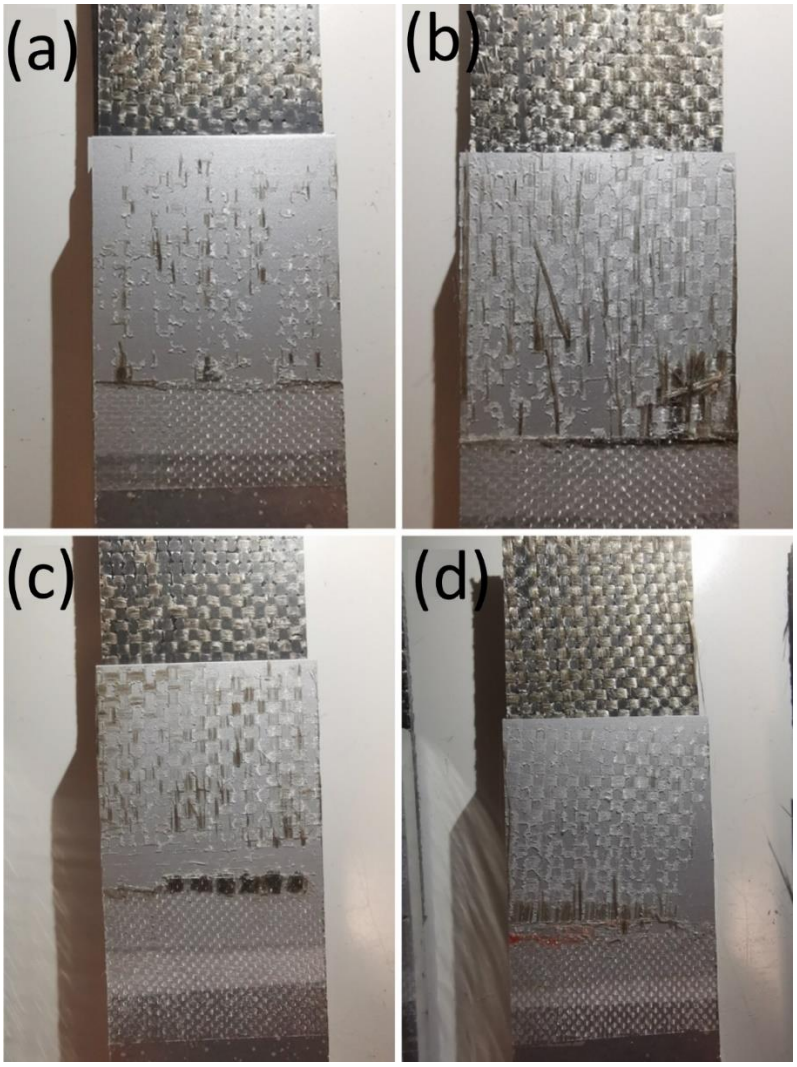

Fig. 14: Typical fracture surfaces of basalt joints: (a) TSA-TT-SIL, (b) TSA-ACE-SIL, (c) TSA-NaOH-TT-SIL, (d) TSA-NaOH-ACE-SIL

4 Conclusions

The present paper deals with the optimization of mechanical response and corrosion resistance of adhesive joints between aluminium alloy 5083 and fibre (i.e., basalt or glass) reinforced epoxy composite substrates. To this scope, the metal alloy was treated with the process of tartaric sulfuric acid (TSA) anodizing in order to evaluate for the first time its effect on the joint performances. Furthermore, a post-immersion in NaOH solution of some TSA anodized samples was carried out. As regards the composite substrate, a silane treatment was carried out on glass and basalt fibres to improve the fibre-matrix adhesion thus further increasing the overall mechanical response of the joint.

It was clearly shown that anodizing of AA5083 in TSA solution allows the growth of anodic layers with nanoscopic pores, able to improve the corrosion resistance of the alloys in highly aggressive chloride environment as well as to improve the adhesion with the composite substrate. Indeed, the polarization resistance grew by two orders of magnitude and the joint shear strength by about 50-60% (depend on glass or basalt fibre) compared to reference (i.e. MA). Furthermore, the alkaline etching in NaOH solution widens the pores leading to further enhance the resin uptake and, as a consequence, the resin interlocking (i.e. increment of about 83% of joint shear strength compared to MA, when basalt fibres were used) without compromising the corrosion resistance.

In addition, the silane treatment process had a beneficial effect on the fibre-matrix adhesion in the composite substrate thus resulting in a further improvement of the mechanical response of the joint, regardless of the fibre used as reinforcement phase (i.e., glass or basalt).

Overall, it was shown that the alternative anodizing process based on environmental friendly chromium-free electrolytes (i.e., TSA) can be considered a useful method to obtain metal to composite adhesive joints with higher mechanical strength (i.e., up to + 130% in comparison to the reference joint) as well as improved corrosion resistance.

Acknowledgments

This work was supported by Project ‘‘THALASSA – TecHnology And materials for safe Low consumption And low life cycle cost veSSels And crafts” (PON ‘‘R&C” 2014/2020).

The authors thank CALEF consortium for suppling aluminium alloy sheets.

References

[1] Valenza A, Fiore V, Fratini L. Mechanical behaviour and failure modes of metal to composite adhesive joints for nautical applications. Int J Adv Manuf Technol 2011;53:593–600. https://doi.org/10.1007/s00170-010-2866-1.

[2] Fiore V, Alagna F, Di Bella G, Valenza A. On the mechanical behavior of BFRP to aluminum AA6086 mixed joints. Compos Part B Eng 2013. https://doi.org/10.1016/j.compositesb.2012.12.009.

[3] Mariam M, Afendi M, Abdul Majid MS, Ridzuan MJM, Gibson AG. Tensile and fatigue properties of single lap joints of aluminium alloy/glass fibre reinforced composites fabricated with different joining methods. Compos Struct 2018;200:647–58. https://doi.org/10.1016/j.compstruct.2018.06.003.

[4] Shivakumar KN, Swaminathan G, Sharpe M. Carbon/vinyl ester composites for enhanced performance in marine applications. J Reinf Plast Compos 2006;25:1101–16. https://doi.org/10.1177/0731684406065194.

[5] Fiore V, Calabrese L, Proverbio E, Passari R, Valenza A. Salt spray fog ageing of hybrid composite/metal rivet joints for automotive applications. Compos Part B Eng 2017;108:65–74. https://doi.org/10.1016/j.compositesb.2016.09.096.

[6] Lambiase F, Ko DC. Feasibility of mechanical clinching for joining aluminum AA6082-T6 and Carbon Fiber Reinforced Polymer sheets. Mater Des 2016. https://doi.org/10.1016/j.matdes.2016.06.061.

[7] Fiore V, Alagna F, Galtieri G, Borsellino C, Di Bella G, Valenza A. Effect of curing time on the performances of hybrid/mixed joints. Compos Part B Eng 2013;45:911–8. https://doi.org/10.1016/j.compositesb.2012.05.016.

[8] Bodjona K, Lessard L. Hybrid bonded-fastened joints and their application in composite structures: A general review. J Reinf Plast Compos 2016.

https://doi.org/10.1177/0731684415627296.

[9] Liu Y, Zhuang W. Self-piercing riveted-bonded hybrid joining of carbon fibre reinforced polymers and aluminium alloy sheets. Thin-Walled Struct 2019;144:106340. https://doi.org/10.1016/j.tws.2019.106340.

[10] Campbell FC. Adhesive Bonding and Integrally Cocured Structure: A Way to Reduce Assembly Costs through Parts Integration. Manuf Process Adv Compos 2004:241–301. https://doi.org/10.1016/b978-185617415-2/50009-5.

[11] Cicala G, Pergolizzi E, Piscopo F, Carbone D, Recca G. Hybrid composites manufactured by resin infusion with a fully recyclable bioepoxy resin. Compos Part B Eng 2018;132:69–76. https://doi.org/10.1016/j.compositesb.2017.08.015.

[12] Fiore V, Scalici T, Di Bella G, Valenza A. A review on basalt fibre and its composites. Compos Part B Eng 2015;74:74–94. https://doi.org/10.1016/j.compositesb.2014.12.034.

[13] Asadi A, Baaij F, Mainka H, Rademacher M, Thompson J, Kalaitzidou K. Basalt fibers as a sustainable and cost-effective alternative to glass fibers in sheet molding compound (SMC). Compos Part B Eng 2017;123:210–8. https://doi.org/10.1016/j.compositesb.2017.05.017.

[14] Kwakernaak A, Hofstede J, Poulis J, Benedictus R. Improvements in bonding metals for aerospace and other applications. Woodhead Publishing Limited; 2012. https://doi.org/10.1533/9780857095169.2.235.

[15] Banea MD, Da Silva LFM. Adhesively bonded joints in composite materials: An overview. Proc Inst Mech Eng Part L J Mater Des Appl 2009;223:1–18. https://doi.org/10.1243/14644207JMDA219.

[16] Shang X, Marques EAS, Machado JJM, Carbas RJC, Jiang D, da Silva LFM. Review on techniques to improve the strength of adhesive joints with composite adherends. Compos Part B Eng 2019;177:107363. https://doi.org/10.1016/j.compositesb.2019.107363.

[17] Aghamohammadi H, Eslami-Farsani R, Tcharkhtchi A. The effect of multi-walled carbon nanotubes on the mechanical behavior of basalt fibers metal laminates: An experimental study.

Int J Adhes Adhes 2020. https://doi.org/10.1016/j.ijadhadh.2019.102538.

[18] Keshavarz R, Aghamohammadi H, Eslami-Farsani R. The effect of graphene nanoplatelets on the flexural properties of fiber metal laminates under marine environmental conditions. Int J Adhes Adhes 2020. https://doi.org/10.1016/j.ijadhadh.2020.102709.

[19] Mehr ME, Aghamohammadi H, Abbandanak SNH, Aghamirzadeh GR, Eslami-Farsani R, Siadati SMH. Effects of applying a combination of surface treatments on the mechanical behavior of basalt fiber metal laminates. Int J Adhes Adhes 2019. https://doi.org/10.1016/j.ijadhadh.2019.04.015.

[20] Gonzalez-Canche NG, Flores-Johnson EA, Cortes P, Carrillo JG. Evaluation of surface treatments on 5052-H32 aluminum alloy for enhancing the interfacial adhesion of thermoplastic-based fiber metal laminates. Int J Adhes Adhes 2018;82:90–9. https://doi.org/10.1016/j.ijadhadh.2018.01.003.

[21] Park SY, Choi WJ, Choi HS, Kwon H, Kim SH. Recent trends in surface treatment technologies for airframe adhesive bonding processing: A review (1995-2008). J Adhes 2010;86:192–221. https://doi.org/10.1080/00218460903418345.

[22] Aghamohammadi H, Hosseini Abbandanak SN, Eslami-Farsani R, Siadati SMH. Effects of various aluminum surface treatments on the basalt fiber metal laminates interlaminar adhesion. Int J Adhes Adhes 2018;84:184–93. https://doi.org/10.1016/j.ijadhadh.2018.03.005.

[23] Di Franco F, Zaffora A, Santamaria M, Di Quarto F. Anodization and anodic oxides. Elsevier Inc.; 2018. https://doi.org/10.1016/B978-0-12-409547-2.11704-4.

[24] Diggle JW, Downie TC, Goulding CW. Anodic oxide films on aluminum. Chem Rev 1969;69:365–405. https://doi.org/10.1021/cr60259a005.

[25] Saenz de Miera M, Curioni M, Skeldon P, Thompson GE. Modelling the anodizing behaviour of aluminium alloys in sulphuric acid through alloy analogues. Corros Sci 2008;50:3410–5. https://doi.org/10.1016/j.corsci.2008.09.019.

[26] Elabar D, La Monica GR, Santamaria M, Di Quarto F, Skeldon P, Thompson GE. Anodizing

of aluminium and AA 2024-T3 alloy in chromic acid: Effects of sulphate on film growth. Surf Coatings Technol 2017;309:480–9. https://doi.org/10.1016/j.surfcoat.2016.11.108.

[27] Zhang J-S, Zhao X-H, Zuo Y, Xiong J-P. The bonding strength and corrosion resistance of aluminum alloy by anodizing treatment in a phosphoric acid modified boric acid/sulfuric acid bath. Surf Coatings Technol 2008;202:3149–56. https://doi.org/10.1016/j.surfcoat.2007.10.041.

[28] Curioni M, Skeldon P, Koroleva E, Thompson GE, Ferguson J. Role of Tartaric Acid on the Anodizing and Corrosion Behavior of AA 2024 T3 Aluminum Alloy. J Electrochem Soc 2009;156:C147. https://doi.org/10.1149/1.3077602.

[29] Dunwoody BJ, Stracey RJ. Superplastic forming of aluminium alloys. vol. 5. Woodhead Publishing Limited; 1989. https://doi.org/10.1533/9780857092779.3.247.

[30] Ferreira DP, Cruz J, Fangueiro R. Surface modification of natural fibers in polymer composites. Green Compos. Automot. Appl., 2018. https://doi.org/10.1016/B978-0-08-102177-4.00001-X.

[31] España JM, Samper MD, Fages E, Sánchez-Nácher L, Balart R. Investigation of the effect of different silane coupling agents on mechanical performance of basalt fiber composite laminates with biobased epoxy matrices. Polym Compos 2013. https://doi.org/10.1002/pc.22421.

[32] Kuzmin KL, Timoshkin IA, Gutnikov SI, Zhukovskaya ES, Lipatov Y V., Lazoryak BI. Effect of silane/nano-silica on the mechanical properties of basalt fiber reinforced epoxy composites. Compos Interfaces 2017;24:13–34. https://doi.org/10.1080/09276440.2016.1182408.

[33] Yu S, Oh KH, Hwang JY, Hong SH. The effect of amino-silane coupling agents having different molecular structures on the mechanical properties of basalt fiber-reinforced polyamide 6,6 composites. Compos Part B Eng 2019;163:511–21. https://doi.org/10.1016/j.compositesb.2018.12.148.

[34] Calabrese L, Bonaccorsi L, Capri A, Proverbio E. Effect of silane matrix on corrosion

protection of zeolite based composite coatings. Metall Ital 2014;106:35–9.

[35] Ma Y, Zhou X, Thompson GE, Curioni M, Hashimoto T, Skeldon P, et al. Anodic Film Formation on AA 2099-T8 Aluminum Alloy in Tartaric–Sulfuric Acid. J Electrochem Soc 2011;158:C17. https://doi.org/10.1149/1.3523262.

[36] Jenkins PG, Yang L, Liggat JJ, Thomason JL. Investigation of the strength loss of glass fibre after thermal conditioning. J Mater Sci 2015;50:1050–7. https://doi.org/10.1007/s10853-014-8661-x.

[37] Mahltig B. Basalt fibers. Inorg Compos Fibers Prod Prop Appl 2018:195–217. https://doi.org/10.1016/B978-0-08-102228-3.00009-8.

[38] Sabet SMM, Akhlaghi F, Eslami-Farsani R. The effect of thermal treatment on tensile properties of basalt fibers. J Ceram Sci Technol 2015;6:245–8. https://doi.org/10.4416/JCST2014-00053.

[39] Thomason JL. Glass fibre sizing: A review. Compos Part A Appl Sci Manuf 2019;127. https://doi.org/10.1016/j.compositesa.2019.105619.

[40] Tourlonias M, Bueno MA, Jordan C, Poquillon D. Influence of Wear on the Sizing Layer and Desizing of Single Carbon Fibre-to-Fibre Friction. Wear 2018. https://doi.org/10.1016/j.wear.2018.02.003.

[41] Deák T, Czigány T, Tamás P, Németh C. Enhancement of interfacial properties of basalt fiber reinforced nylon 6 matrix composites with silane coupling agents. Express Polym Lett 2010;4:590–8. https://doi.org/10.3144/expresspolymlett.2010.74.

[42] Rita S, Eti R, Tetty K. Aminopropyltrimethoxysilane (APTMS) modified nano silica as heavy metal iron (Fe) adsorbents in peat water. AIP Conf Proc 2018;2014. https://doi.org/10.1063/1.5054567.

[43] Rudzinski S, Häussler L, Harnisch CH, Mäder E, Heinrich G. Glass fibre reinforced polyamide composites: Thermal behaviour of sizings. Compos Part A Appl Sci Manuf 2011;42:157–64. https://doi.org/10.1016/j.compositesa.2010.10.018.

Figure captions

Table Captions